Classical Dynamics Study of the Unimolecular Decomposition of CH_3SH^+

Emilio Martínez-Núñez* and Saulo A. Vázquez

Departamento de Química Física, Universidad de Santiago de Compostela, Santiago de Compostela E−15706, Spain

Received: June 30, 1999; In Final Form: September 8, 1999

The dynamics of three decomposition channels of the mercapto cation (CH_3SH^+) were investigated by classical trajectories and RRKM formalisms. The three channels are (I) CH bond dissociation through a "tight" transition state, (II) CS bond cleavage, and (III) SH bond scission. These calculations were performed with an analytical potential energy surface constructed from theoretical and experimental data available in the literature. The relative yields of CH_3^+ and CH_2SH^+ products are in qualitative agreement with charge-exchange experiments. The dynamical calculations revealed that the system is intrinsically non-Rice−Ramsperger−Kassel−Marcus (RRKM) at the energies selected in this study. Under nonrandom initial conditions, the system showed strong mode specificity, which may be rationalized by weak couplings between the low- and high-frequency modes, particularly the CH_3 stretching normal modes, which is consistent with collisional activation studies. The classical trajectory calculations revealed an inverse isotope effect for both the CS and SH scission channels and a normal isotope effect for the CH bond dissociation process. Finally, we have found that molecular rotation decreases the mercapto cation decomposition rate and that orbital angular momentum dramatically modifies the relative yields of CH_3^+ and CH_2SH^+ products.

Introduction

The mercapto cation (CH_3SH^+) has been the focus of several experimental[1−12] and theoretical[13−16] studies over the last years. The rearrangement and fragmentation reactions involving this species have been explored by several experimental techniques: collisional activation,[1] mass spectrometry,[2,6,9] charge exchange,[10] and photoelectron−photoion coincidence (PEPICO).[11] In the recent collisional activation experiment,[1] the C−S bond dissociation to form CH_3^+ and SH was found to be the dominant product channel, even though this reaction channel is not among the energetically preferred pathways. In other words, the dissociation dynamics of CH_3SH^+ via collisional activation was found to be nonstatistical. Fenn et al.[1] attributed the high yield of $CH_3^+ + SH$ "to the more efficient translational to vibrational energy transfer for the C−S stretch than for the C−H stretches of CH_3SH^+, and to weak couplings between the low-frequency C−S and the high-frequency C−H stretching vibrational modes of CH_3SH^+". In contrast, the breakdown diagrams of CH_3SH^+ obtained in the charge-exchange,[10] PEPICO,[11] and photoionization mass spectrometric[9] experiments agree qualitatively with that predicted by Rice−Ramsperger−Kassel−Marcus (RRKM) calculations.[9]

Motivated by such evidence for nonstatistical behavior, we performed classical trajectory and RRKM calculations for three decomposition channels of the mercapto cation:

$$CH_3SH^+ \rightarrow CH_2SH^+ + H \quad \text{(I)}$$

$$CH_3SH^+ \rightarrow CH_3^+ + SH \quad \text{(II)}$$

$$CH_3SH^+ \rightarrow CH_3S^+ + H \quad \text{(III)}$$

Reaction channels II and III are simple bond fission processes involving "loose" transition states, whereas reaction I evolves through a critical structure (a "tight" transition state). Reaction I is the most favorable channel among those indicated above because the critical energy for this process is 25−30 kcal/mol[1,13] below the critical energies for reactions II and III.

Our study began with the construction of a realistic potential energy surface (PES) based on available experimental[17−19] and theoretical[13] data and flexible enough to model the three decomposition channels. We then employed our PES to calculate microcanonical rate constants for each channel at several energies and to investigate whether nonstatistical behavior could be exhibited. The role of anharmonicity in the mercapto cation decomposition was assessed by using several RRK schemes that incorporate anharmonic corrections to the microcanonical rate constants. The possibility of mode-specific chemistry was investigated by the calculation of rate constants under selective excitations of vibrational normal modes. The influence of deuterium substitution on the reaction rates was examined by classical trajectory simulations and classical harmonic RRKM theory. Finally, rotational effects were explored for various rotational angular momentum orientations. The results of our classical simulations were compared with charge-exchange[10] and collisional activation studies.[1]

Potential Energy Surface

The general expression of the analytical PES reads

$$V = V(R_{SH}) + V(R_{CS}) + \sum_{i=1}^{3} V(R_{CH(i)}) + V(\theta_{CSH}) + \sum_{i=1}^{3} V(\theta_{SCH(i)}) + \sum_{i=1}^{3}\sum_{j=i+1}^{3} V(\theta_{H(i)CH(j)}) + \sum_{i=1}^{3}\sum_{j=i+1}^{3} V(\omega_{SCH(i)H(j)}) + V(\omega_{H(1)CH(2)H(3)}) + \sum_{i=1}^{3} V(\tau_{HCSH(i)}) \quad (1)$$

where the subscripts i and j refer to the hydrogen atoms (1−3)

10.1021/jp992243n CCC: $18.00
Published on Web 11/13/1999

attached to the carbon atom. Following is a detailed description of the different terms composing our PES.

The sulfur−hydrogen interaction $V(R_{SH})$ is described by a Morse function:

$$V(R_{SH}) = D_{SH}\{1 - \exp[-\alpha_{SH}(R_{SH} - R_{SH,eq})]\}2 - D_{SH} \quad (2)$$

where D_{SH} is the potential well depth and α_{SH} is the curvature parameter of the SH bond. We varied the SH bond length parameter as follows:

$$R_{SH,eq} = R^r_{SH} - (R^r_{SH} - R^p_{SH})SW1 \quad (3)$$

where

$$SW1 = 1 - \exp\{-C_1[R_{CS} - R_{CS,eq}]^2\} \quad (4)$$

The superscripts p and r denote equilibrium values for the product SH and the reactant, respectively. The switching function SW1 was added to alter the SH bond length parameter from that of the reactant to that appropriate for the product SH.

$V(R_{CS})$ is the carbon−sulfur interaction term taken as

$$V(R_{CS}) = D_{CS}\{1 - \exp[-\alpha_{CS}(R_{CS} - R_{CS,eq})]\}^2 - D_{CS} \quad (5)$$

where

$$R_{CS,eq} = R^r_{CS} - (R^r_{CS} - R^p_{CS})SW2 \quad (6)$$

with

$$SW2 = 1 - \exp\{-C_2[R_{CHav} - R^r_{CHav}]^2\} \quad (7)$$

R^r_{CS} and R^p_{CS} are the CS equilibrium geometries of CH_3SH^+ and CH_2SH^+, respectively. To take into account the shift of the CS stretching frequency from the reactant to the product CH_2SH^+, the parameter α_{CS} was varied according to

$$\alpha_{CS} = \alpha^r_{CS} + (\alpha^p_{CS} - \alpha^r_{CS})SW3 \quad (8)$$

where

$$SW3 = 1 - \exp\{-C_3[R_{CHav} - R^r_{CHav}]^2\} \quad (9)$$

In the above expressions, we have introduced a geometric variable R_{CHav} that reflects a weighted contribution from each of the CH bond distances and is defined as

$$R_{CHav} = \sum_{i=1}^{3} R_{CH(i)}s(i) \quad (10)$$

where

$$s(i) = \prod_{\substack{j=1 \\ j\neq i}}^{3}\{0.5[1 - \tanh(a[R_{CH(j)} - R_{CH(i)}])]\} \quad (11)$$

The function $s(i)$ ensures that the major contribution to the sum in eq 10 comes from the longest CH(i) distance. R^r_{CHav} is the value of R_{CHav} calculated by using the geometry of the reactant.

The carbon−hydrogen interaction terms read

$$V(R_{CH(i)}) = D_{CH(i)}\{1 - \exp[-\alpha_{CH(i)}(R_{CH(i)} - R_{CH,eq})]\}^2 - D_{CH(i)} \quad (12)$$

where

$$\alpha_{CH(i)} = \alpha^r_{CH} + (\alpha^p_{CH} - \alpha^r_{CH})SW4 \quad (13)$$

and

$$SW4 = 1 - \exp\{-C_4[R_{CHav} - R^r_{CHav}]^2\} \quad (14)$$

For the sake of simplicity, we employed the same parameter value $R_{CH,eq}$ for all of the CH bonds in the reactant and products.

Bending interactions are described by harmonic functions:

$$V(\theta) = 0.5K_\theta(\theta - \theta_{eq})^2 \quad (15)$$

The force constant for the CSH bending was modeled as follows,

$$K_{CSH} = \{K^r_{CSH} + [K^p_{CSH} - K^r_{CSH}]SW5\}SW6 \times SW7 \quad (16)$$

where

$$SW5 = 1 - \exp\{-C_5[R_{CHav} - R^r_{CHav}]^2\} \quad (17)$$

$$SW6 = \exp\{-C_6[R_{CS} - R_{CS,eq}]^2\} \quad (18)$$

and

$$SW7 = \exp\{-C_6[R_{SH} - R_{SH,eq}]^2\} \quad (19)$$

By means of SW6 and SW7, the CSH bending term vanishes as the CS or SH bond dissociates. On the other hand, SW5 changes the value of the force constant to that appropriate for the product CH_2SH^+.

SCH(i) bending force constants were attenuated by

$$K_{SCH(i)} = K^r_{SCH}SW6 \times W8(i) \quad (20)$$

with

$$SW8(i) = \exp\{-C_7[R_{CH(i)} - R_{CH,eq}]^2\} \quad (21)$$

and

$$\theta_{SCH,eq} = \theta^r_{SCH} + (\theta^p_{SCH} - \theta^r_{SCH})SW9 \quad (22)$$

where

$$SW9 = 1 - \exp\{-C_8[R_{CHav} - R^r_{CHav}]^2\} \quad (23)$$

Switching functions SW6 and SW8 make SCH bends weaken as reaction I or II takes place. Because the SCH(i) bond angles change significantly from the reactant to the product CH_2SH^+, we have included the function SW9 to change adequately the $\theta_{SCH,eq}$ bond angle parameter.

Force constants for the three H(i)CH(j) bends have the form

$$K_{H(i)CH(j)} = \{K^r_{HCH} - [K^r_{HCH} - K^p_{HCH}]SW10\}SW8(i) \times SW8(j) \quad (24)$$

where

$$SW10 = 1 - \exp\{-C_9[R_{CHav} - R^r_{CHav}]^2\} \quad (25)$$

and

$$\theta_{HCH,eq} = \theta^r_{HCH} + (\theta^p_{HCH} - \theta^r_{HCH})SW11 \quad (26)$$

where

$$SW11 = 1 - \exp\{-C_{10}[R_{CS} - R_{CS,eq}]^2\} \quad (27)$$

If H(i) or H(j) takes part in the CH bond scission process, the bending term vanishes according to SW8. On the other hand, if the other hydrogen atom is involved in the CH dissociation, SW10 changes the value of the force constant to that appropriate for the product CH_2SH^+. SW11 was employed to change the value of the HCH equilibrium bond angle as reaction II evolves.

The wagging interaction in the product CH_2SH^+ was modeled by

$$\sum_{i=1}^{3}\sum_{j=1+1}^{3} V(\omega_{SCH(i)H(j)}) = \sum_{i=1}^{3}\sum_{j=i+1}^{3} 0.5K_{SCH(i)H(j)}[\omega_{SCH(i)H(j)}]^2 \quad (28)$$

The wagging force constant $K_{SCH(i)H(j)}$ was varied by the switching function SW8,

$$K_{SCH(i)H(j)} = K^{p1}_{\omega}[1 - SW8(k)] \quad (29)$$

where k^{p1}_{ω} is the wagging force constant for the product CH_2SH^+. The wagging term concerning the product CH_3^+ is

$$V(\omega_{H(1)CH(2)H(3)}) = 0.5K_{H(1)CH(2)H(3)}[\omega_{H(1)CH(2)H(3)}]^2 \quad (30)$$

where

$$K_{H(1)CH(2)H(3)} = K^{p2}_{\omega}\{1 - \exp[-C_{11}(R_{CS} - R_{CS,eq})^2]\} \quad (31)$$

and K^{p2}_{ω} is the wagging force constant for the product CH_3^+.

Explicitly, $V(\tau_{HCSH(i)})$ in eq 1 is written as

$$V(\tau_{HCSH(i)}) = \sum_{j=0}^{5} a_{j,HCSH(i)} \cos(j\tau) + \sum_{j=0}^{5} b_{j,HCSH(i)} \cos(j\tau) \quad (32)$$

The first sum on the right-hand side of eq 32 concerns the torsion around the C−S bond in CH_3SH^+, whereas the second sum refers to CH_2SH^+. The torsional coefficients $a_{j,HCSH(i)}$ were attenuated as follows:

$$a_{j,HCSH(i)} = a^r_j SW12 \times SW13 \times SW7 \quad (33)$$

with

$$SW12 = \exp\{-C_{12}[R_{CS} - R_{CS,eq}]^2\} \quad (34)$$

and

$$SW13 = \exp\{-C_{13}[R_{CHav} - R^r_{CHav}]^2\} \quad (35)$$

where a^r_j are the torsional coefficients for the reactant CH_3SH^+. The coefficients $b_{j,HCSH(i)}$ depend on the hydrogen atom H(i) and have the following form,

$$b_{j,HSCH(i)} = b^p_j[1 - SW13][1 - s(i)] \quad (36)$$

with b^p_j being the torsional coefficients for the product CH_2SH^+.

Table 1 collects geometrical features, frequencies, and relative energies obtained from the literature,[13,17−19] and the corresponding values computed by means of GENDYN code[20] and our model PES. All of the parameters of our PES are listed in Table 2. The equilibrium bond distances and angles were taken from ab initio structures optimized at the QCISD/6-311G** level of theory.[13] Force constants, curvature parameters, potential well depths, and parameters C_1−C_{13} were fitted to reproduce more accurately the geometries, frequencies, and energetics available in the literature.[13,17−19]

A comparison of equilibrium geometries, energies, and vibrational frequencies computed by our PES with the corresponding ab initio and experimental values shows reasonable agreement (see Table 1). More specifically, for geometries, it can be seen that the structural parameters at the reactant conformation (CH_3SH^+) calculated by the analytical PES are in nearly exact accord with the ab initio values. For the transition state, the major differences involve the bond that is being broken. Thus, deviations of 0.117 Å appear for the C−H equilibrium bond length, and a difference of 5.6° appears for the H−CS equilibrium bond angle. On the other hand, the relative energies computed by our PES agree very well with the literature values. The barrier height for reaction I is computed to be 55.98 kcal/mol by our PES, a value similar to that predicted by ab initio theory (55.15 kcal/mol).[13] The reaction endothermicities predicted by our model PES for reactions II and III are 85.81 and 81.0 kcal/mol, respectively, which compare quite well with the ab initio figures (85.77 and 80.4 kcal/mol, respectively).[13] Finally, the vibrational frequencies computed numerically by the analytical potential are in general agreement with the ab initio frequencies evaluated at the MP2/6-311G** level of accuracy.

Dynamical Study

A. Computational Methods. *1. Trajectory Calculations.* We have performed classical trajectory simulations, employing the GENDYN code,[20] at energies ranging from 100 to 170 kcal/mol. The initial conditions for the computations were established in one of the following ways.

The first method to assign initial conditions was the efficient microcanonical sampling (EMS)[21] with the angular momentum restricted to zero. This method is based on a Monte Carlo "random walk" technique for microcanonical sampling of coordinates and momenta, which generates a random distribution of energy over the entire molecule. The sampling was carried out by performing a Markov walk in configuration space, with all of the Cartesian coordinates being varied 0.10 Å. This selection was made to achieve an acceptance ratio of about 0.5 for the Markov chain. During the incubation period, 50 000 steps were made, and the final configuration was used as the "starting geometry" of the molecule. Initial momenta were then generated from the appropriate microcanonical distribution so that the required total energy was obtained. Maximum bond extensions allowed during the random walk to confine the sampling to reactant configuration space were 2 Å for all of the bonds. The angular momentum was restricted in the initial condition selections of these ensembles because we wanted to make these calculations comparable to those in which normal modes are selectively excited.

In the second method, vibrational quanta were assigned to each normal mode with random vibrational phases. A total energy of 140 kcal/mol was allocated among the vibrational modes in such a way that one mode was initially excited and the remaining modes contained the zero-point vibrational energy.

For trajectories incorporating molecular rotation, we assigned initial conditions as follows. We first distributed 130 kcal/mol

TABLE 1: Equilibrium Geometries, Energetics, and Frequencies for the Chemical Species Involved in This Study[a]

internal	CH_3SH^+		TS		CH_2SH^++H		CH_3^++SH			CH_3S^++H		
coord.	PES[b]	ref 13[c]	PES[b]	ref 13[c]	PES[b]	ref 13[c]	PES[b]	exp.[d]	ref 13[c]	PES[b]	exp.[e]	ref 13[c]
SH	1.351	1.351	1.351	1.348	1.351	1.349	1.343	1.352	1.343			
CS	1.799	1.799	1.633	1.638	1.628	1.628				1.799	1.767	1.771
CH_1	1.090	1.096	1.090	1.088	1.090	1.088	1.090	1.087	1.094	1.090		1.098
CH_2	1.090	1.090	2.292	2.175			1.090	1.087	1.094	1.090		1.098
CH_3	1.090	1.090	1.090	1.088	1.090	1.089	1.090	1.087	1.094	1.090		1.098
CSH	97.6	97.6	97.6	97.7	97.6	97.9						
H_1CS	108.2	107.8	120.3	122.7	122.5	122.9				108.2		108.3
H_2CS	108.2	108.4	104.2	109.8						108.2		108.3
H_3CS	108.2	108.4	120.3	117.5	122.5	117.6				108.2		108.3
H_1CH_2	110.7	111.3	86.1	83.1			120.0		120.0	110.7	102.5	110.4
H_1CH_3	110.7	111.3	119.0	119.5	115.0	119.4	120.0		120.0	110.7	102.5	110.4
H_2CH_3	110.7	109.4	85.5	83.0			120.0		120.0	110.7	102.5	110.4
H_1CSH	180.0	180.0	176.7	177.1	0.0	0.0						
H_2CSH	60.0	59.3	3.7	4.2								
H_3CSH	−60.0	−59.3	−89.4	−90.5	180.0	180.0						

Harmonic Frequencies/(cm^{-1})

descr.[f]	PES[b]	ref 13[c]	PES[b]	ref 13[c]	PES[b]	ref 13[c]	PES[b]	exp.[d]	ref 13[c]	PES[b]	exp.[e]	ref 13[c]
torsion	233	230	525i	761i	825	873	1141		1448	715		754
CS str.	697	727	327	387	1019	905	1453		1453	1117		881
CSH bend	787	820	362	423	1123	1078	1453		1453	1120		881
CH_3 rock	1117	882	812	866	1264	1102	3301		3093	1392		1368
CH_3 rock	1122	1130	994	950	1524	1152	3491		3303	1392		1401
CH_3 bend	1392	1376	1009	1046	1713	1507	3491		3303	1536		1401
CH_3 bend	1392	1447	1256	1156	2552	2740				3220		3034
CH_3 bend	1536	1453	1336	1169	3380	3174	2552		2800	3341		3147
SH str.	2552	2736	1745	1511	3489	3300				3341		3147
CH_3 str.	3220	3069	2552	2758								
CH_3 str.	3341	3162	3360	3175								
CH_3 str.	3341	3234	3486	3299								

Relative Energy/(kcal/mol)

PES[b]	ref 13[c]	PES[b]	ref 13[c]	PES[b]	ref 13[c]	PES[b]	exp.[d]	ref 13[c]	PES[b]	exp.[e]	ref 13[c]
0.0	0.0	55.98	55.15	54.37	54.02	85.81		85.77	81.0		80.4

[a] Distances given in angstroms and angles in degrees. [b] This study. [c] QCISD(T)/6-311G** and MP2/6-311G** data from Martínez-Núñezand Vázquez.[13] [d] Taken from Crofton et al.[17] and Ashfold et al.[18] [e] Taken from Hsu et al.[19] [f] Approximate description of the normal modes at the reactant geometry.

into vibration according to the EMS algorithm. Then, the molecule was positioned in the principal axes of inertia. The required initial rotational energy was then specified together with the direction cosines defining L_a:L_b:L_c, where L_i is the ith component of rotational angular momentum, defined with respect to the principal axes of inertia. In our calculations we employed a rotational energy of 10 kcal/mol.

The lifetime of a trajectory resulting in reaction I was taken to be the integration time up to the point at which the system reaches the top of the barrier: $R_{CH} > 2.292$ Å; R_{CH^*}, $R_{CH^{**}}$, R_{CS}, and $R_{SH} < 2$ Å, where the star and double star denote the hydrogen atoms that remain attached to the carbon atom. However, to check for immediate recrossings of the transition state, the trajectory was followed until the CH distance were greater than 5 Å. The lifetime of the trajectories resulting in reactions II and III was taken to be the integration time up to the last inner turning point of the CS and SH vibrations, respectively. However, trajectories that had not undergone at least one CS or SH vibration were not included in the ensemble averages.

Trajectories of both types of initial conditions were integrated by using a fourth-order Runge−Kutta−Gill routine. The determination of the step size for numerical integration has been done by trial and error on the basis of accuracy requirements. The value 0.08 fs has been found to be sufficient to warrant conservation of energy to better than four significant figures. Typically, an ensemble comprised 2000 trajectories, with each trajectory being followed until a bond dissociation had occurred (CH, CS, or SH distance greater than 5 Å) or 10 ps had elapsed.

RRKM theory assumes that the unimolecular decomposition is statistical with the probability that decomposition occurs in the time interval t to $t + dt$ given by the lifetime distribution

$$P(t) = -\frac{1}{N(0)}\frac{dN(t)}{dt} = k(E)\exp[-k(E)t] \qquad (37)$$

where $k(E)$ is the RRKM rate constant. When a microcanonical statistical method is employed to initialize the trajectories, the $t = 0$ intercept of $P(t)$ gives the anharmonic RRKM rate constant, which will be called $k_{RRKM}^{traj}(E)$. In addition, the total rate constant involving the three channels investigated here is $k_{CH} + k_{CS} + k_{SH}$, where k_{CH}, k_{CS}, and k_{SH} are the individual rates for the CH, CS, and SH bond cleavage, respectively.

2. Statistical Calculations. The microcanonical RRKM rate constant of a unimolecular reaction can be expressed as the flux across a dividing surface (transition state) separating reactants and products[22]

$$k(E) = \frac{1}{2}\frac{\int d\Gamma \delta[H(\Gamma) - E]\delta(q_{RC} - q_C)|\dot{q}_{RC}|}{\int d\Gamma \delta[H(\Gamma) - E]} \qquad (38)$$

where Γ is the complete set of position and momentum coordinates $\{\mathbf{q}, \mathbf{p}\}$, $H(\Gamma)$ is the Hamiltonian of the system

TABLE 2: Parameters for the Analytical PES

Stretching Parameters

parameter	value[a]	parameter	value[b]	parameter	value[c]
R^r_{SH}	1.351	α_{SH}	1.83	D_{SH}	81.00
R^p_{SH}	1.343	α^r_{CS}	1.62	D_{CS}	85.80
R^r_{CS}	1.799	α^p_{CS}	2.25	D_{CH}	54.00
R^p_{CS}	1.628	α^r_{CH}	2.70		
		α^p_{CH}	2.82		

Bending Parameters

parameter	value[d]	parameter	value[e]
θ_{CSH}	97.6	K^r_{CSH}	0.60
θ^r_{SCH}	108.2	K^p_{CSH}	0.70
θ^p_{SCH}	120.0	K^r_{SCH}	0.90
θ^r_{HCH}	110.7	K^r_{HCH}	0.43
θ^p_{HCH}	120.0	K^p_{HCH}	0.23

Wagging Parameters

parameter	value[e]
K^{p1}_{ω}	0.50
K^{p2}_{ω}	0.25

Torsional Parameters[f]

a^r_0	a^r_1	a^r_2	a^r_3	a^r_4	a^r_5
0.0084	0	0	0.0084	0	0
b^p_0	b^p_1	b^p_2	b^p_3	b^p_4	b^p_5
0.50	0	−0.50	0	0	0

Switching Functions Parameters

parameter	value[g]	parameter	value[g]	parameter	value[b]
C_1	1.00	C_9	0.0001	a	100
C_2	2.50	C_{10}	1.00		
C_3	2.50	C_{11}	0.50		
C_4	3.60	C_{12}	1.00		
C_5	1.00	C_{13}	0.91		
C_6	1.00				
C_7	0.96				
C_8	0.84				

[a] In angstroms. [b] In inverse angstroms. [c] In kilocalorie/mole. [d] In degrees. [e] In millidyn angstrom per square radian. [f] In electronvolts. [g] In inverse square angstroms.

excluding the center of mass motion, $q_{RC} = q_{RC}(\mathbf{q})$ is the reaction coordinate, q_C is the critical value of q_{RC} required for reaction, and $\dot{q}_{RC} = \dot{q}_{RC}(\mathbf{q})$ is the velocity through the critical surface. The integrals over Γ in eq 38 are understood to be over the reactant part of phase space.

Equation 38 may be rewritten in a form suitable to be evaluated by EMS algorithms:

$$k(E) = \frac{1}{2}\frac{\int d\mathbf{q} W(\mathbf{q}) \delta(q_{RC} - q_C) \langle|\dot{q}_{RC}|\rangle}{\int d\mathbf{q} W(\mathbf{q})} \tag{39}$$

In this equation, $W(\mathbf{q})$ is the statistical weight of configuration $\mathbf{q}$:

$$W(\mathbf{q}) = (I_a I_b I_c)^{-1/2}[E - V(\mathbf{q})]^{(3N-8)/2} \tag{40}$$

where $I_a I_b I_c$ is the product of the principal moments of inertia and N is the total number of atoms. $\langle|\dot{q}_{RC}|\rangle$ is the average absolute velocity along the reaction coordinate, given by

$$\langle|\dot{q}_{RC}|\rangle = \frac{\int d\mathbf{p} \delta[T(\mathbf{p}) - K]|\dot{q}_{RC}|}{\int d\mathbf{p} \delta[T(\mathbf{p}) - K]} \tag{41}$$

where $K = E - V(\mathbf{q})$ is the kinetic energy at configuration $\mathbf{q}$ and $T(\mathbf{p})$ is the kinetic energy for momentum $\mathbf{p}$.

It is common to introduce an importance sampling function $I(\mathbf{q})$, with the same form as the EMS weight, to increase the convergence rate:

$$I(\mathbf{q}) = (I_a I_b I_c)^{-1/2}[E - V(\mathbf{q})]^{\alpha} \tag{42}$$

where α is an adjustable parameter. This yields an effective weight factor of

$$W_{eff}(\mathbf{q}) = (I_a I_b I_c)^{-1/2}[E - V(\mathbf{q})]^{[(3N-8)/2]-\alpha} \tag{43}$$

Good convergence in the calculation of the rate constant may be achieved when the exponent in eq 43 takes a value between 1 and 1.5.[23,24] Consequently, in our study, we selected $\alpha = 4$. Hereafter, the RRKM rate constant thus determined will be referred to as $k^{stat}_{RRKM}(E)$.

The statistical rate constant $k^{stat}_{RRKM}(E)$ is an upper limit to the "true" rate constant computed by classical trajectories $k^{traj}_{RRKM}(E)$ on the same potential energy surface.[25] Consequently, the value of $k^{stat}_{RRKM}(E)$ should be minimized with respect to the location of the transition-state dividing surface. Details of the minimization procedure are given elsewhere.[23]

For the special case of simple bond scissions, the average absolute velocity across the transition-state dividing surface has been evaluated analytically[23] by the formula

$$\langle|\dot{q}_{RC}|\rangle = (2K/\pi\mu)^{1/2}\frac{[(3N-5)/2]!}{[(3N-4)/2]!} \tag{44}$$

where μ is the reduced mass for motion along the reaction coordinate.

For the CH, CS, and SH bond scissions, the reaction coordinates q_{RC} were the lengths of the dissociating bonds so that the dividing surfaces were spheres of radii equal to q_C. An incubation period of 5×10^4 random moves was first performed and then a Markov walk of 3×10^7 steps was completed in the reactant region of the PES. At each step of the Markov walk, all of the atoms were moved 0.10 Å. We considered 7, 12, and 11 transition-state dividing surfaces (separated by 0.1 Å) for reaction channels I, II, and III, respectively. The statistical RRKM rates reported in this study are the average of eight values of the rate constant with different initial random number seeds.

B. Results and Discussion. *1. EMS Initial Conditions.* When the EMS scheme is used to excite the mercapto cation, the lifetime distributions were found to be biexponential at all of the energies selected here. For the sake of example, the lifetime distributions obtained at 120 and 150 kcal/mol are illustrated in Figures 1 and 2, respectively. The biexponential decay indicates that the decomposition is intrinsically non-RRKM,[26,27] with only the intercept of $P(t)$ being equal to the microcanonical RRKM rate constant. Table 3 summarizes the nonexponential characteristics of the lifetime distributions and product branching ratios following EMS initialization. It is clearly seen that most of the reactive trajectories resulted in CH bond scission, as expected on account of the lower energy barrier for this process. The trajectory branching ratios k_{CS}/k_{CH} and k_{SH}/k_{CH} indicate that CS and SH bond scissions become more probable as the energy increases. Particularly, k_{CS}/k_{CH} increases significantly from 0.01 to 0.1 (in the energy range 110−170 kcal/mol), and k_{SH}/k_{CH} increases from 0.01 to 0.02 (in the energy range 120−170 kcal/mol). As the energy rises, the entropy factor is larger, and therefore, reactions II and III, which involve loose transition

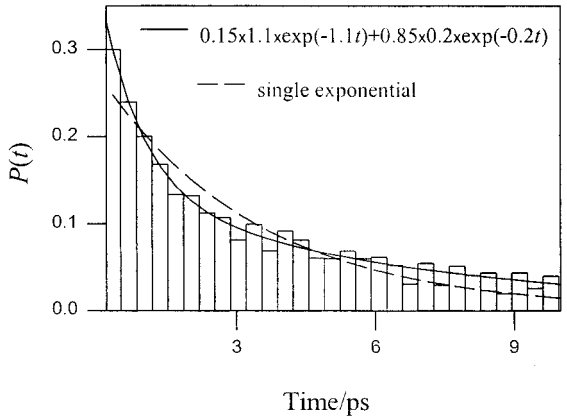

Figure 1. Lifetime distribution of the mercapto cation at 120 kcal/mol when the trajectories were initialized using the EMS scheme. The initial decay rate is ≈0.3 ps^{-1}, whereas the rates associated with the biexponential are 1.1 and 0.2 ps^{-1}. The single-exponential fit is also shown for comparison.

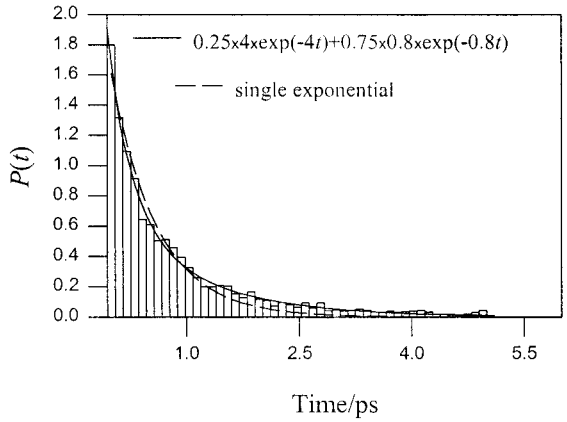

Figure 2. Lifetime distribution as in Figure 1 but at an energy of 150 kcal/mol. In this case, the initial decay rate is ≈0.8 ps^{-1}, and the rates associated with the biexponential are 4 and 0.8 ps^{-1}. The single-exponential fit is also shown for comparison.

TABLE 3: Rate Constants and Product Branching Ratios from Trajectory Simulations of the Mercapto Cation Decomposition

			branching ratios	
energy[a]	rate constants[b]	$k^{traj}_{RRKM}(E)$[c]	k_{CS}/k_{CH}	k_{SH}/k_{CH}
100	0.3 (2%), 0.03 (98%)	0.03	[d]	[e]
110	1.1 (5%), 0.1 (95%)	0.1	0.01	[e]
120	1.1 (15%), 0.2 (85%)	0.3	0.03	0.01
130	3.3 (15%), 0.4 (85%)	0.5	0.07	0.01
140	3.1 (30%), 0.4 (70%)	1.1	0.09	0.01
150	4.1 (25%), 0.8 (75%)	1.8	0.12	0.01
160	6.9 (25%), 2.0 (75%)	2.7	0.14	0.02
170	12.1 (25%), 1.9 (75%)	4.3	0.11	0.02

[a] In kilocalorie per mole. [b] The percentage of trajectories decaying with a certain rate constant is given in parentheses. [c] Intercept of $P(t)$ following EMS initialization. [d] At this energy, no CS dissociations were observed in the simulation period of time. [e] At this energy, no SH dissociations were observed in the simulation period of time.

states, become important. On the other hand, even though the critical energies for reactions II and III are very similar, reaction II is markedly faster than reaction III.

As pointed out above, the statistical rate constants should be minimized with respect to the location of the dividing surface to obtain the correct microcanonical rate. For the CH bond cleavage, the minimum in the k-versus-q_C profile was found in the range 2.1−2.3 Å, moving inward slowly as energy increases. For the CS and SH bond rupture processes, the minima were located at larger distances (between 3.1 and 3.3 Å for the CS dissociation and between 3.5 and 3.8 for the SH dissociation). The RRKM rate constants and product branching ratios calculated by means of EMS algorithms $k^{stat}_{RRKM}(E)$ are given in Table 4. A comparison of the classical microcanonical RRKM rate constants determined from the $P(t)$ intercept (and listed in Table 3) with the statistical RRKM rate constants listed in Table 4 shows reasonable agreement. Particularly for the three lowest energies, $k^{stat}_{RRKM}(E)$ is equal to $k^{traj}_{RRKM}(E)$. For energies between 130 and 170 kcal/mol, the statistical rates are about 1.1−1.2 times higher than the trajectory rates. It must be stressed that for a rigorous comparison the definition of the transition state used in the statistical and trajectory calculations should be identical. In the statistical calculations, the rate is determined by the first passage of a trajectory through the dividing surface. However, transition-state recrossings are allowed in the trajectory simulations. We therefore performed additional trajectory calculations, at 120 and 170 kcal/mol, in which the transition-state definition resembles that in the statistical calculations. At 120 kcal/mol, recrossings have a very minor effect on the decay rate. When determining the decomposition rates from the first time at which the mercapto cation crosses one of the dividing surfaces at 120 kcal/mol, the decay remains double exponential with 20% of the trajectories reacting with a rate constant of 1.1 ps^{-1} and 80% with a rate constant of 0.2 ps^{-1}. The $t = 0$ intercept of $P(t)$ is 0.3 ps^{-1}. These results are very similar to those obtained when recrossings are taken into account (see Table 3). However, at 170 kcal/mol, the effect of recrossings is more significant. Thus, the trajectory results in which the lifetime was taken to be the time up to the first passage of the dividing surface show biexponential decay with 25% of the trajectories decaying with a rate constant of 13 ps^{-1} and the remaining 75% with a rate constant of 2 ps^{-1}. In addition, the RRKM rate constant determined from the $P(t)$ intercept is 4.6 ps^{-1}, which is equal to the statistical rate constant (4.6 ± 0.1 ps^{-1}).

On the other hand, the product branching ratios determined from statistical calculations are in close agreement with the trajectory results, indicating that the CH bond scission channel is the preferred one, with the CS and SH channels being more important as the energy increases.

To examine the extent of anharmonicity in the microcanonical rate constants, we used several RRK schemes, recently proposed by Song and Hase.[28] The classical harmonic RRKM expression read

$$\log k(E) = \log \nu + (s - 1) \log[(E - E_0)/E] \qquad (45)$$

s where E_0 is the barrier height for the process, s is the total number of degrees of freedom among which the total energy E is assumed to be randomized, and ν is[29]

$$\nu = \frac{\prod_{i=1}^{s} \nu_i}{\prod_{j=1}^{s-1} \nu_j} \qquad (46)$$

with ν_i and ν_j being the reactant and transition-state harmonic vibrational frequencies, respectively. It is very common to fit this expression to trajectory rate constants, even though eq 46 is only exact for a harmonic Hamiltonian. To introduce anharmonicity into the RRK expression, one has to make the ν term energy-dependent. In addition, variational effects, which

TABLE 4: Statistical RRKM Rate Constants (ps^{-1}) for the Decomposition of the Mercapto Cation[a]

energy[b]	$k^{stat}_{RRKM}(E)$	k_{CH}	k_{CS}	k_{SH}	k_{CS}/k_{CH}	k_{SH}/k_{CH}
100	0.03 ± 0.004	0.03 ± 0.004	$5 \times 10^{-5} \pm 1 \times 10^{-5}$	$1 \times 10^{-5} \pm 4 \times 10^{-6}$	0.001	2×10^{-4}
110	0.12 ± 0.009	0.12 ± 0.008	0.002 ± 0.0007	$2 \times 10^{-4} \pm 6 \times 10^{-5}$	0.02	0.002
120	0.31 ± 0.01	0.30 ± 0.01	0.01 ± 0.004	$0.001 \pm 3 \times 10^{-4}$	0.04	0.005
130	0.61 ± 0.03	0.55 ± 0.02	0.05 ± 0.01	0.01 ± 0.005	0.07	0.02
140	1.33 ± 0.05	1.22 ± 0.03	0.09 ± 0.01	0.02 ± 0.007	0.08	0.02
150	2.10 ± 0.07	1.91 ± 0.04	0.16 ± 0.02	0.03 ± 0.01	0.08	0.02
160	3.12 ± 0.1	2.73 ± 0.06	0.32 ± 0.04	0.07 ± 0.01	0.11	0.02
170	4.60 ± 0.1	4.02 ± 0.09	0.49 ± 0.04	0.13 ± 0.02	0.12	0.03

[a] Errors associated are 95% confidence limits. [b] Energy is in kilocalorie per mole.

are very important for the CS and SH bond cleavages, make E_0 energy-dependent. Thus, the RRK expression, modified to incorporate the above effects, becomes

$$\log k(E) = \log \nu(E) + (s-1)\log[(E - E_0(E))/E] \quad (47)$$

In this work, and following Song and Hase,[28] the potential energy at the variational transition state E_0 for reactions II and III was approximated by

$$E_0(E) = D_0 - cE_\infty \quad (48)$$

where $E_\infty = E - D_0$ is the energy in excess of the dissociation energy D_0. On the other hand, $\nu(E)$ may be modeled by

$$\nu(E) = af_{anh}(E) \quad (49)$$

where the constant a represents the energy-independent harmonic factor and $f_{anh}(E)$ is an anharmonic correction term. We considered two different RRK schemes. The anharmonic correction term in the two schemes reads[28]

$$f_{anh}(E) = \frac{\exp[b^{ts}(E - E_0)]}{\exp(bE)(1 + bE/s)} \quad (50)$$

where two different parameters b and b^{ts} were considered for the reactant and transition state, respectively.

Schemes 1 and 2 differ in the treatment of the degrees of freedom of the CS and SH transition states. In scheme 1, all of the transition-state degrees of freedom were considered as vibrations, and therefore, eq 47 applies. In scheme 2, some motions were treated as rotors, as described below. The well-known RRKM expression is

$$k(E) = \frac{W^{ts}(E^*)}{h\rho(E)} \quad (51)$$

where $\rho(E)$ is the density of states of the reactant molecule and $W^{ts}(E^*)$ is the total number of states on the transition-state surface (with energy $E^* = E - E_0$).[29] The dissociation reactions involve "loose" transition states. In such cases, the motions of the fragments about axes perpendicular to the breaking bond are relatively unhindered and may conveniently be treated as two-dimensional rotors.[30] In the model we use here, the reactant rocking modes become two-dimensional free rotors at the transition state. The density of states for the two two-dimensional rotors is:

$$\rho^{rot}(E) = \frac{E}{B_1B_2} \quad (52)$$

where B_1 and B_2 are the rotational constants for the two-dimensional motions around axes perpendicular to the reaction coordinate. Thus, the total sum of states at the transition state

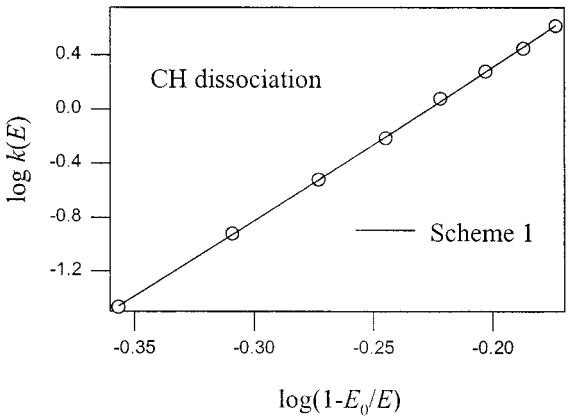

Figure 3. Microcanonical rate constants for the CH dissociation channel obtained by RRKM theory with our potential energy surface (circles) and fitted RRK rates according to scheme 1.

can be written as a convolution of the classical vibrational sum of states W^v at the transition state and the density of states of the two two-dimensional rotors:

$$W^{ts}(E^*) = \int_0^{E^*} W^{\nu}(E_+)\rho^{rot}(E^* - E_+)\, dE_+ \quad (53)$$

Then, the rate constant becomes

$$k(E) = \frac{\nu h^4 (s-1)(s-2)}{B_1B_2} \frac{(E - E_0)^{s-3}}{E^{s-1}} \quad (54)$$

In this case, ν does not include the transition-state frequencies related to the two-dimensional rotors. Scheme 2 uses this rate constant expression with the aforementioned anharmonic and variational corrections. This scheme was applied to reaction channels II and III.

In the fits, the number of vibrational degrees of freedom s was set to 12. The classical threshold energies D_0 were set to the values obtained by our potential energy surface (see Table 1). As shown in Figures 3−5, the trajectory rates (circles, triangles, or squares) are well-fitted by either scheme 1 or 2. However, for CS and SH bond dissociation channels, the best fits were achieved by scheme 2. In other words, the treatment of several degrees of freedom at the transition state as two-dimensional rotors rather than vibrations leads to the best agreement between statistical RRKM and trajectory results. The results of the fits are given in Table 5. The anharmonic corrections to the reactant's density of states at the threshold varies between 2 and 26, depending on the reaction channel and scheme used. These results suggest that anharmonicity plays an important role in the evaluation of the microcanonical rate constants at the range of energies investigated.

2. Normal/Local Mode Excitations. To explore the possibility of mode-specific effects, we have also evaluated the trajectory rates and branching ratios resulting from initial excitation of

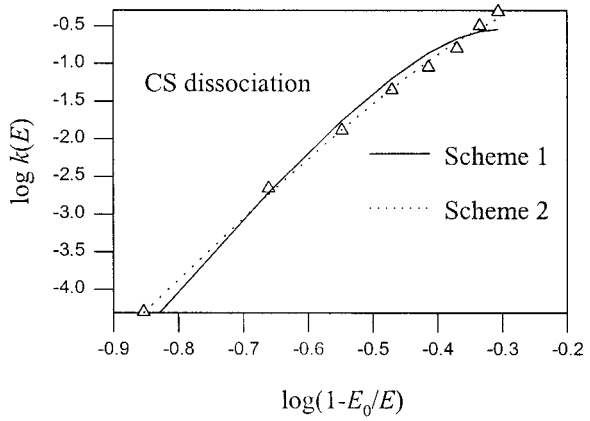

Figure 4. Comparison of two fits to the CS dissociation rate constants: △, microcanonical RRKM rates; −, RRK scheme 1; and - - -, RRK scheme 2.

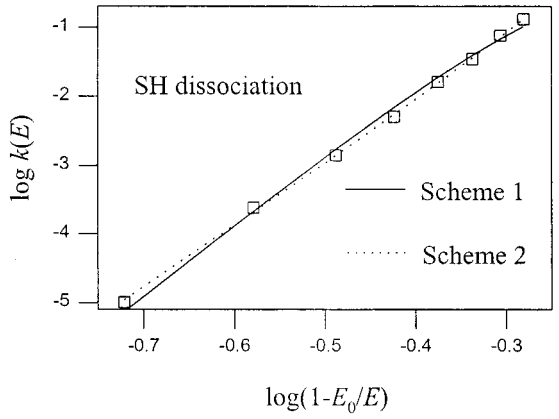

Figure 5. Comparison of two fits to the SH dissociation rate constants: △, microcanonical RRKM rates; −, RRK scheme 1, and (- - -) RRK scheme 2.

each normal mode at 140 kcal/mol. Hereafter, each ensemble will be denoted by the frequency (in inverse centimeters) of the normal mode initially excited, and normal modes will also be distinguished by their frequencies (in inverse centimeters) at the reactant geometry. For an approximate description of each normal mode at the equilibrium geometry, see Table 1.

The trajectory rates and product branching ratios obtained from trajectory simulations are collected in Table 6 for those ensembles in which normal modes were initially excited. For the ensemble in which the SH stretch was initially excited, all of the trajectories decayed within 0.005 ps, and neither CH nor CS bond dissociations occurred. Overall, the computed results shown in Table 6 indicate a high degree of mode-specific chemistry. The branching ratios show that excitations of the three lowest frequency modes (233, 697, and 787), closely related to the torsion, the CS stretch, and the CSH bend, respectively, enhance the CS and SH bond scission rates. In particular, ensembles 697 and 787 yield the highest k_{CS}/k_{CH} branching ratios and ensembles 787 and 2552 clearly favor the SH bond dissociation process. On the contrary, excitations of CH_3 stretching modes enhance the rate of reaction I as could be expected.

To complete the previous analysis, we have monitored the local mode energies at a total energy of 60 kcal/mol, just above the CH dissociation threshold, for ensembles of 100 trajectories in which either the SH or the CH local mode was initially excited. Figure 6 displays graphically the average (CH, CS, and SH) mode energies of an ensemble in which one CH bond is initially excited. As seen in this figure, there is an irreversible and complete energy leakage from the initially excited CH mode in 0.6 ps. The other two CH modes gain energy due to strong couplings between the three CH stretches, whereas the SH mode and the low-frequency CS mode do not significantly participate in the vibrational relaxation. On the other hand, Figure 7 depicts the average mode energies for an ensemble in which the SH bond is initially excited. The behavior of this ensemble is completely different from that in Figure 6. In this case, the SH bond energy is localized in this mode during the 5 ps of simulation. Neither the CH nor the CS mode gains energy in this period of time. This behavior indicates that the SH mode acts as an intramolecular bottleneck for IVR (intramolecular vibrational energy redistribution).

3. Isotope Effects. One of the purposes of this study was to analyze the influence of deuterium substitution on the rates of reactions I−III. To this end, we performed classical trajectory calculations under microcanonical (EMS) initial conditions for the decomposition of CH_3SH^+, CH_2DSH^+, CHD_2SH^+, CD_3SH^+, and CD_3SD^+, constraining the total angular momentum to zero in order to facilitate a further comparison with classical harmonic RRKM predictions. The ratios k_H/k_D [where k_H and k_D stand for the rates of the undeuterated and deuterated molecules, respectively], calculated by trajectory simulations at 140 kcal/mol, are shown in Table 7. The rates were computed from the $t = 0$ intercept of $P(t)$ to make a direct comparison with classical harmonic RRKM rates. We found that upon deuterium substitution the global rate and the CH dissociation rate diminish (normal isotope effect), but the CS (for three and four deuterium atoms) and SH dissociation rates increase (inverse isotope effect).

To evaluate the classical harmonic RRKM rates for reaction I, we employed eq 45. Consequently, the RRKM computed ratio can be obtained by

$$\frac{k_H}{k_D} = \frac{\nu_H}{\nu_D} \tag{55}$$

As seen in Table 7, trajectory and RRKM calculations predict a normal isotope effect with the ratios k_H/k_D in reasonable agreement.

For reactions II and III, which involve loose transition states, we employed eq 54, and then the ratio k_H/k_D reads

$$\frac{k_H}{k_D} = \frac{(B_1B_2)_D}{(B_1B_2)_H}\frac{\nu_H}{\nu_D} \tag{56}$$

For the CS scission channel, the ratio k_H/k_D determined by classical harmonic RRKM theory with the above expressions led to values close to unity. For CD_3SH^+ and CD_3SD^+, the trajectory results predict an inverse isotope effect for reaction II; for the latter species, the RRKM prediction is in agreement. However, when the statistical uncertainties in the trajectory calculations and the approximations inherent in the above expressions are taken into account, these results should be taken with caution.

For reaction channel III, the transition state has one two-dimensional rotor, so that eq 56 becomes:

$$\frac{k_H}{k_D} = \frac{B_D}{B_H}\frac{\nu_H}{\nu_D} \tag{57}$$

The RRKM computed ratios agree in general with those obtained by the trajectory calculations, predicting an inverse isotope effect for the four species.

TABLE 5: Fits to Microcanonical Rate Constants with Modified RRKM Schemes[a]

channel	scheme	D_0	a	b	b^{ts}	c	$f_{anh,\rho}(E_0)$[b]	fit[c]
I	1	56	2.9×10^5	5.4×10^{-2}	5.2×10^{-2}	-	26	1.02
II	1	86	9.6×10^7	3×10^{-2}	2.7×10^{-3}	1.9×10^{-3}	16	1.42
II	2	86	1×10^8	7.7×10^{-3}	4.1×10^{-5}	4.5×10^{-2}	2	1.13
III	1	81	2.9×10^3	9.7×10^{-3}	1.3×10^{-5}	7.3×10^{-2}	2	1.22
III	2	81	9.4×10^7	3.2×10^{-2}	4×10^{-2}	4×10^{-2}	16	1.06

[a] The units for the parameters are kilocalorie per mole for D_0, picoseconds^{-1} for a, inverse kilocalorie per mole for b and b^{ts}, and c is unitless. [b] Anharmonic correction to the reactant's density of states at the unimolecular threshold. [c] Average of the ratios between the microcanonical and fitted rate constants. For each point, the rate constant ratio used is the one greater than unity.

TABLE 6: Trajectory Rate Constants (ps^{-1}) and Branching Ratios for Normal Mode Excitations[a]

ensemble[c]	rate constants	k_{CS}/k_{CH}	k_{SH}/k_{CH}
233	[b]	0.06	0.2
697	2.2 (40%), 0.02 (60%)	1.4	0.05
787	10.1 (82.5%), 0.3 (17.5%)	0.6	5
1117	3.3 (60%), 0.8 (40%)	0.05	0.001
1122	3.1 (65%), 0.7 (35%)	0.05	0.001
1393	3.9 (55%), 0.8 (45%)	0.06	0.001
1393	4.1 (60%), 0.8 (40%)	0.05	0.002
1537	6.2 (40%), 0.9 (60%)	0.06	0.001
2552	[b]	[c]	[c]
3221	9.9 (60%), 0.9 (40%)	0.04	0.0007
3341	31.0 (90%), 0.3 (10%)	0.01	0.0004
3342	9.2 (60%), 0.9 (40%)	0.04	0.0007

[a] In these calculations, the total energy was 140 kcal/mol. [b] For these ensembles, we were unable to fit the trajectory results to a biexponential. [c] For this ensemble, we only observed SH bond dissociations.

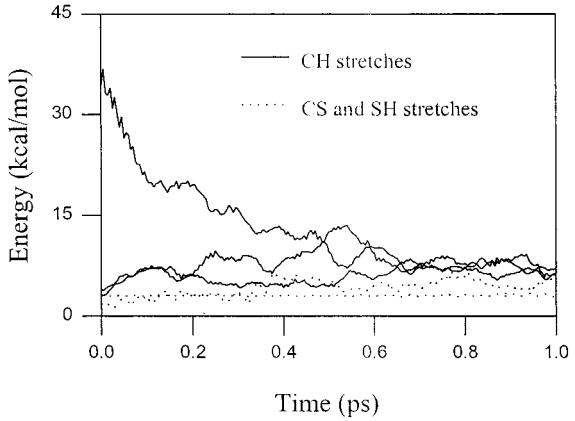

Figure 6. Mode energies averaged over 100 trajectories for an ensemble in which a CH bond is initially excited.

For both reaction channels II and III, the inverse isotope effect may arise from the presence of two-dimensional rotations at the transition state, which provides a much larger sum of states contribution in the deuterated species than that in CH_3SH^+. However, it must be stressed that for the CD_3SD^+ species in reaction III primary and secondary isotope effects may be involved. Primary isotope effects generally have two contributing components: the so-called "statistical weight" effect, arising from changes in densities of states upon isotopic substitution, and the "critical energy" effects, arising from the difference in zero-point energies in the SD and SH bonds.[29,31] Our classical trajectory and classical RRKM calculations display only the purely mass-dependent, statistical weight contribution to the isotope effect. Therefore, the inverse isotope effect found for the CD_3S^+-D dissociation could be overestimated in the present calculations.

4. The Influence of Molecular Rotation on the Mercapto Cation Decomposition. As Fenn et al.[1] indicated, the initial energy distribution in their experiment could involve the rotational degrees of freedom. We therefore investigated the influence of molecular rotation and angular momentum orientation on the decay rates of CH_3SH^+. Three orientations of the angular momentum were considered lying parallel to the three principal axes of inertia. The initial reactant vibrational energy was randomly distributed among the vibrational degrees of freedom. The resulting rate constants are listed in Table 8. As seen in the table, molecular rotation decreases the microcanonical rate constant substantially as is suggested by RRKM theory. Therefore, it seems that rotation is inactive for randomization of energy. However, it must be stressed that *b*- and *c*-axes excitations substantially increase the ratio k_{CS}/k_{CH}.

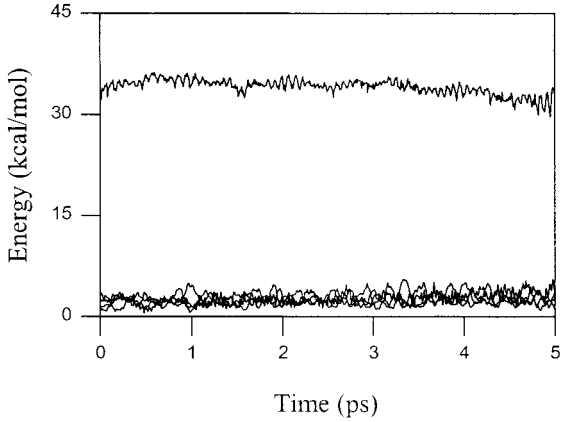

Figure 7. Mode energies averaged over 100 trajectories for an ensemble in which a SH bond is initially excited.

TABLE 7: Microcanonical Rate Constants (ps^{-1}) and Ratios k_H/k_D for Decomposition of CDH_2SH^+, CD_2HSH^+, CD_3SH^+, and CD_3SD^+ at 140 Kcal/mol

	k_H/k_D[a]			
molecule	global	channel I	channel II	channel III
CDH_2SH^+	1.20	1.23 (1.01)	1.12 (1.05)	0.65 (0.86)
CD_2HSH^+	1.24	1.27 (1.53)	1.12 (1.07)	0.61 (0.76)
CD_3SH^+	1.30	1.38 (1.49)	0.90 (1.09)	0.78 (0.69)
CD_3SD^+	1.53	1.62 (1.44)	0.90 (0.97)	0.80 (0.69)

[a] EMS initial conditions were employed in the trajectory calculations. Values in parentheses correspond to the classical harmonic RRKM computations.

TABLE 8: Rate Constants and Product Branching Ratios from Trajectory Simulations of Rotating Mercapto Cation[a]

			branching ratios[b]	
excitation	rate constants[c]	$k_{RRKM}^{traj}(E)$[d]	k_{CS}/k_{CH}	k_{SH}/k_{CH}
a-axis	1.6 (30%), 0.4 (70%)	0.8	0.03	0.01
b-axis	1.0 (30%), 0.3 (70%)	0.5	0.19 (4.8)	0.01[e]
c-axis	1.8 (15%), 0.3 (85%)	0.6	0.20	0.01

[a] An energy of 140 kcal/mol was employed in these computations. [b] Values in parentheses correspond to initial excitation of the CS stretch with 10 kcal/mol added to *b*-axis rotation. [c] The percentage of trajectories decaying with a certain rate constant is given in parentheses. [d] Intercept of $P(t)$ following EMS initialization. [e] For this ensemble, no SH dissociations were observed in the simulation period of time.

The mercapto cation is a nearly symmetric top at the reactant geometry with principal moments of inertia: $I_a = 5.01$ amu Å^{-2}, $I_b = 38.19$ amu Å^{-2}, and $I_c = 39.97$ amu Å^{-2}. The dependence of the rate constants on the direction of rotational motion may be explained by the effects of the centrifugal force. For L_b and L_c excitations, the centrifugal force nearly lies on the CS bond, and therefore, the effect of rotational motion is to enhance the CS dissociation channel. The rotational energy associated with excitation of the orbital angular momentum is channeled into the CS dissociation reaction coordinate as the two moieties separate.

We also calculated the lifetime distribution for an ensemble in which the CS stretch and orbital angular momentum are excited. In this case, we found a large percentage (≈50%) of trajectories decaying within one vibrational period of the CS reaction coordinate and no SH dissociations in the simulation period of time. Thus, CS dissociations are clearly favored over CH dissociations. In summary, energy placed in specific rotational and vibrational degrees of freedom can dramatically modify the yield of CH_3^+ or CH_2SH^+ products.

5. Comparison to Experiment. It is very interesting to compare our results obtained under statistical initial conditions with those obtained in charge-exchange studies,[10] because as we stated in the Introduction these experiments are in qualitative agreement with RRKM theory. In the energy range 120−145 kcal/mol, a ratio k_{CS}/k_{CH} of ≈0.02 was extracted from the breakdown diagrams of the charge-exchange experiment.[10] This value is somewhat lower than our computed trajectory branching ratios (0.03−0.09) in the same energy range. However, it must be noted that in the experimental work other ions were observed because more channels than those selected here are open at these energies; therefore, the comparison should be taken with caution. On the other hand, the energy randomization assumption seems to be valid in the charge-exchange study because the abundance of product ions observed in the experiment is consistent with RRKM predictions.[9] However, the statistical calculations of Kutina et al.[9] were based on assumed parameters (vibrational frequencies and moments of inertia), so that their conclusions may be questionable. In fact, our classical trajectory results suggest that, in the energy range 100−170 kcal/mol, the mercapto cation behaves nonstatistically.

In the energy range 120−145 kcal/mol, the collisional activation study of Fenn et al.[1] predicted a ratio k_{CS}/k_{CH} of ≈4. In this case, as they pointed out, the initial energy distribution should be nonrandom; that is, the rotational and low-frequency vibrational degrees of freedom are expected to be excited upon collisional activation.[1] In the previous section, we discussed the effects of molecular rotation in the product branching ratios. In particular, we found that excitation of the CS stretch and orbital angular momentum resulted in a ratio k_{CS}/k_{CH} of 4.8. Our results are in agreement with the experiment of Fenn et al.,[1] but comparisons must be taken with care because of the limitations of our potential energy surface and the uncertainty in the initial conditions of the collisional activation studies.[1] Nevertheless, we found weak couplings between the high- (CH stretches) and the low-frequency vibrational modes, as can be extracted from Tables 6 and 8. As a result, if the energy is preferentially deposited in the C−S stretch or orbital angular momentum is excited, the CH_3-SH^+ bond dissociation dominates over the other dissociation process even though the dissociation energy for this process is significantly higher than that for $H-CH_2-SH^+$ cleavage.

Concluding Remarks

We have investigated three unimolecular decomposition channels of the mercapto cation by classical trajectory and statistical methods. These three decomposition channels are the dissociations of bonds CH (I), CS (II), and SH (III). Reaction I proceeds through a transition state, whereas reactions II and III are simple bond scissions.

We have constructed a reliable potential energy function that models the three decomposition channels. With this potential function, we have evaluated rate constants and branching ratios for the unimolecular processes at total energies ranging from 100 to 170 kcal/mol. Under random initial conditions, the branching ratios indicate that reaction I is much faster than reactions II and III and that II is an order of magnitude faster than III. The branching ratio k_{CS}/k_{CH} obtained in this study under statistical initial conditions is in qualitative agreement with the results of charge-exchange experiments.[10] The dynamical calculations suggest that the system is intrinsically non-RRKM at the energies selected in this study. Anharmonicity effects on the decomposition rates were investigated by fitting RRK schemes incorporating anharmonic corrections to the microcanonical rate constants.

The study of normal mode excitations predicts a high degree of mode specificity in the unimolecular channels of CH_3SH^+. This specificity comes from the poor coupling between the low- and the high-frequency vibrational modes (in particular CH_3 stretches), as suggested by Fenn et al.[1] in their collisional activation study. In addition, the SH stretch mode has been found as a bottleneck for IVR.

The trajectory simulations reveal an inverse isotope effect for both the CS and SH scission channels and a normal isotope effect for the CH bond dissociation. The inverse isotope effect could be explained by the presence of two-dimensional rotors at the transition state.

Finally, molecular rotation decreases the decomposition rate, but orbital angular momentum excitation promotes CS bond scissions.

Acknowledgment. We thank R. Rodríguez-Fernández for his help as system manager of our computing facilities. We are pleased to acknowledge financial support of this research from Xunta de Galicia (XUGA20903A98).

References and Notes

(1) Fenn, P. T.; Chen, Y.-J.; Stimson, S.; Ng, C. Y. *J. Phys. Chem. A* **1997**, *101*, 6513.

(2) Amos, D.; Gills, R. G.; Occolowitz, J. L.; Pisani, J. F. *Org. Mass Spectrom.* **1969**, *2*, 209.

(3) (a) Keyes, B. G.; Harrison, A. G. *J. Am. Chem. Soc.* **1968**, *90*, 5671. (b) Harrison, A. G. *J. Am. Chem. Soc.* **1978**, *100*, 4911.

(4) Frost, D. C.; Herring, F. G.; Katrib, A.; McDowell, C. A.; McLean, R. A. N. *J. Phys. Chem.* **1972**, *76*, 1030.

(5) Cradock, S.; Whiteford, P. A. *J. Chem. Soc., Faraday* 2 **1972**, *68*, 281.

(6) (a) Holmes, J. L.; Lossing, F. P.; Terlouw, J. K.; Burgers, P. C. *J. Am. Chem. Soc.* **1982**, *104*, 2931. (b) Terlouw, J. K.; Heerma, W.; Dijkstra, G.; Holmes, J. L.; Burgers, P. C. *Int. J. Mass. Spectrom. Ion Phys.* **1983**, *47*, 147. (c) Holmes, J. L.; Lossing, F. P.; Terlouw, J. K.; Burgers P. C. *Can. J. Chem* **1983**, *61*, 2305.

(7) Kimura, K., Katsumata, S., Achiba, Y., Yamazaki, T., Iwata, S., Eds. *Handbook of Helium I Photoelectron Spectra of Fundamental Organic Molecules*; Halsted: New York, 1981.

(8) Akopyan, M. E.; Serhiev, Y. L.; Vilesov, F. I. *Klim. Vys. Energy* **1970**, *4*, 305.

(9) Kutina, R. E.; Edwards, A. K.; Berkowitz, J. *J. Chem. Phys.* **1974**, *77*, 5508.

(10) Jonsson, B.-Ö.; Lind, J. *J. Chem. Soc., Faraday Trans. 2* **1974**, *70*, 1399.

(11) Nourbakhsh, S.; Norwood, K.; Yin, H.-M.; Liao, C.-L.; Ng, C. Y. *J. Chem. Phys.* **1991**, *95*, 945.
(12) Cheung, Y.-S.; Hsu, C.-W.; Huang, J.-C.; Li, W.-K.; Chiu, S.-W. *Int. J. Mass Spectrom. Ion Processes* **1996**, *13*, 159.
(13) Martínez-Núñez, E.; Vázquez, S. A. *J. Mol. Struct. (THEOCHEM)*, in press.
(14) Chiu, S.-W.; Li, W.-K.; Tzeng, W.-B.; Ng, C. Y. *J. Chem. Phys.* **1992**, *97*, 6557.
(15) Nobes, R. H.; Bouma, W. J.; Radom, L. *J. Am. Chem. Soc.* **1984**, *106*, 2774.
(16) Curtiss, L. A.; Nobes, R. H.; Pople, J. A.; Radom, L. *J. Chem. Phys.* **1992**, *97*, 6766.
(17) Crofton, M. W.; Jagod, M.-F.; Rehfuss, B. D.; Kreiner, W. A.; Oka, T. *J. Chem. Phys.* **1988**, *88*, 666.
(18) Ashfold, M. N.; Tutcher, B.; Western, C. M. *Mol. Phys.* **1989**, *66*, 981.
(19) Hsu, Y.-.C.; Lin, X.; Miller, T. A. *J. Chem. Phys.* **1989**, *90*, 1852.
(20) Thompson, D. L. GENDYN program.
(21) (a) Schranz, H. W.; Nordholm, S.; Nyman, G. *J. Chem. Phys.* **1991**, *94*, 1487. (b) Nyman, G.; Nordholm, S.; Shranz, H. W. *J. Chem. Phys.* **1990**, *93*, 6767.
(22) Doll, J. D. *J. Chem. Phys.* **1980**, *73*, 2760; **1981**, *74*, 1074.
(23) (a) Shranz, H. W.; Raff, L. M.; Thompson, D. L. *J. Chem. Phys.* **1991**, *94*, 4219; (b) *Chem. Phys. Lett.* **1990**, *68*, 171.
(24) Kay, R. D.; Raff, L. M. *J. Phys. Chem. A* **1997**, *101*, 1007.
(25) Pechukas, P. *Annu. Rev. Phys. Chem.* **1981**, *32*, 159.
(26) Bunker, D. L.; Hase, W. L. *J. Chem. Phys.* **1973**, *59*, 4621.
(27) Hase, W. L. In *Dynamics of Molecular Collisions B*; Miller, W. H., Ed.; Plenum: New York, 1976.
(28) Song, K.; Hase, W. L. *J. Chem. Phys.* **1999**, *110*, 6198.
(29) Robinson, P. J.; Holbrook, K. A. *Unimolecular Reactions*; Wiley: New York, 1972.
(30) Gilbert, R. G.; Smith, S. C. *Theory of Unimolecular and Recombination Reactions*; Blackwell Scientific: Oxford, 1990.
(31) Forst, W. *Theory of Unimolecular Reactions*; Academic Press: New York, 1973.